Research Article

Nima Mohammadi Taher, Maedeh Mahmoudi*, and Seyyede Shahrzad Sajjadivand

Cobalt Catalysts Preparation and Characterization over Alumina Support for Fischer Tropsch Synthesis

https://doi.org/10.1515/bfuel-2017-0004
Received Aug 10, 201; accepted Dec 05, 2017

Abstract: An investigation was done to develop and characterize the alumina supported cobalt catalyst for Fischer-Tropsch Synthesis to produce biodiesel from biomass with the aim to produce alumina-supported cobalt catalysts containing 7 to 19 wt.% cobalt content. By using incipient wetness impregnation of γ-Al_2O_3 supports with cobalt nitrate hexahydrate with ethanol and distilled water solutions; the 14 wt.% cobalt content in catalyst was achieved. Nitrogen adsorption-desorption, X-ray diffraction (XRD), scanning electron microscopy (SEM), energy dispersive spectroscopy (EDS), X-ray fluorescence (XRF), H_2temperature programmed reduction (H_2-TPR), temperature programmed desorption (TPD), temperature programmed oxidation (TPO) and carbon monoxide chemisorption were used for the characterization of the catalysts to attain an appropriate cobalt catalyst. In order to investigate the effect of the impregnation on the crystalline size, surface area and cobalt content, three different impregnation methods with various durations were investigated. In addition, increasing the impregnation duration increased the cobalt content and its dispersion. Based on results, positive effect of the alumina support and impregnation duration on the crystallite size, surface area, and pore diameter, reducibility of the catalyst and cobalt dispersion were investigated. Thus, cobalt catalyst for using in fixed bed reactor to produce biodiesel from biomass through Fischer-Tropsch Synthesis was prepared and characterized.

Keywords: Fischer-Tropsch Synthesis; Biodiesel; Narrow pore alumina support; Cobalt catalyst; Ethanol

***Corresponding Author: Maedeh Mahmoudi:** Department of Chemistry, Islamic Azad University (IAU), Tehran North Branch, Tehran, Iran; Email: msh_mahmoudi@yahoo.com
Nima Mohammadi Taher, Seyyede Shahrzad Sajjadivand: Department of Materials Engineering, Faculty of Engineering, University of Tabriz, Tabriz, Iran

1 Introduction

In previous years growing concerns with regards to the fast depletion of fossil energy resources and a need to reduce greenhouse gas emissions make renewable energy sources much more attractive. The Energy concerns in the world and economic growth in the developing countries are dramatically rising [1–11] so, the energy demands in the field of transportation and manufacturing have increased. Also, in the near future biomass is expected to play an important role and it would be one of the important renewable energy sources [2, 8, 9, 12]. Use of Hydrogen is another significant research area in the field of renewable energy [2].

An option for production of renewable fuels from gasified biomass is the Fischer-Tropsch Synthesis (FTS). The Fischer-Tropsch Synthesis is considered as an efficient solution to the problem of finding appropriate substitutes for liquid fossil fuels [3, 9, 13, 14]. Fischer-Tropsch Synthesis is a technology that has an extensive history of gasoline and diesel production from coal and natural gas. The fuel produced by using FTS could be one of the best solutions to the fuels emission due to its high quality [2–6, 9, 13–15]. FTS technology devised nearly 90 years ago by Franz Fischer and Hans Tropsch in Germany. Equation 1 represents the main reaction in FTS in which syngas (hydrogen and carbon monoxide) is converted to long chain Hydrocarbons over cobalt catalysts during the reaction

$$n\ (\mathrm{CO} + 2\mathrm{H_2}) \rightarrow (-\mathrm{CH_2}-)_n + n(\mathrm{H_2O}) \qquad (1)$$

FTS is a surface polymerization reaction in which the reaction between CO and H_2 takes place on the surface of the cobalt catalysts. This process is described as a Carbide formation on the surface of the catalysts which was discovered by Fischer and Tropsch nine decades ago [9]. They assumed that the carbide carbons are decomposed by hydrogen with regeneration of the catalysts metal and can be transformed to hydrocarbons. CH_2 entities are formed on the surface of the catalyst and arranged in a row on the surface which implies the carbide mechanism [16]. An-

other assumption is the free movement of CH_X units along the catalyst. Two other reactions occur after a hydrocarbon molecule is released from the catalyst surface and reabsorbed to follow other reaction paths. Methane formation as an unwanted product in FTS is shown in the equation 2 and 3 in which is considered as an irreversible reaction. The other important reaction which occurs in the FTS process is a water gas shift reaction that produces water as co product; this reaction plays a vital role in reactors which reaction take place over cobalt catalysts and produce carbon dioxide as an undesirable by-product [4, 17].

$$(CO + 3H_2) \rightarrow (CH_4) + (H_2O) \tag{2}$$

$$(CO + H_2O) \leftrightarrow (CO_2) + (H_2) \tag{3}$$

Catalysts, reaction conditions, the type of reactor and H_2/CO ratio all have an influence on the type of products generated through FTS. Chain growth probability is affected by catalyst selection for FTS mechanism, which influences product distribution. Cobalt (Co), iron (Fe), nickel (Ni) and ruthenium (Ru) are the main catalysts which are used for a FT synthesis process. The high cost of Ruthenium forces it to be ignored for use in industrial application. Nickel is not feasible for FT process due to very low average molecular weight of this material [18]. In FTS process the Water Gas Shift Reaction (WGSR) activity over iron catalyst is more than cobalt catalyst and it can lead to loss of carbon monoxide as a raw gas by formation of carbon dioxide within WGSR. Water as co-product of this process can be produced by the activity of WGSR which is kinetic inhibition of this catalyst. Lower activity of methane formation reaction in cobalt based catalytic reactors result in higher selectivity of liquid products. Cobalt catalyst is active at low temperature which makes it appropriate to produce biodiesel at low temperature and has durability on stream of up to 5 years compared to 6 months in the case of iron catalyst. Chain growth probability is 0.5-0.7 for iron catalyst and 0.7-0.8 for cobalt catalyst. For cobalt catalyst chain growth probability can be maximizing up to value of 0.95 [19].

A cobalt catalyst is considered as a proficient and capable catalyst for the production of biodiesel from biomass through FTS because of its high activity at low temperature [15, 20]. Cobalt based catalysts are able to produce a high yield in the production of long chain synthesis hydrocarbon. FTS process over cobalt catalyst at normal pressure and temperature of 200-300°C produces linear α olefins (C_nH_{2n}) as the main product and a small amount of nonlinear products which contain mono methyl branch compounds. Also, it was considered that increasing the residence time in reactor lead to secondary reactions with the same skeleton of both products, subsequent hydrogenation of olefins formed paraffin (C_nH_{2n+2}). High pressure Fischer Tropsch Synthesis over cobalt catalyst produces less olefin in favor of Alkane (C_nH_{2n+2}) content due to the increase of the molecular weight. FTS in fixed bed reactor over iron catalysts produces Naphthenes ($C_{10}H_8$) and aromatics in small amounts; however none of these compounds are usually produced over cobalt and ruthenium catalysts [21].

In comparison with iron and ruthenium catalysts, cobalt catalyst have a low rate of carbon monoxide activation, with low hydrogenolysis and a low shift activity at high H_2/CO ratio; make it reasonable to produce synthetic diesel production (Fe<Co<Ru). Cobalt catalysts have high hydrogenation activity when alkanes are preferred as the main product (Fe<Co<Ru). This catalyst is not affected by stream practically [22]. It can conclude that cobalt supported catalysts have been mostly appropriate for the production of biodiesel in the low temperature FTS process because of their higher productivity and hydrocarbon selectivity at lower pressure and temperature and low water gas shift activity and stability toward deactivation by water [23].

Physical properties of the catalyst are influenced by the type of the support selected for catalyst production. Surface area, pore volume and pore size distribution of the support have an important effect on the characterization of the catalyst as a high surface area improves the metal dispersion and reparation which increases the exposure of cobalt to gaseous reactants [24]. Al_2O_3, TiO_2, SiO_2 and MgO are the common supports that are utilized for cobalt catalyst production. Constructive mechanical properties of alumina make this support suitable to prepare cobalt catalyst for FTS process [24, 25]. Cobalt oxides species crystalline sizes are influenced by pore size and distribution. Xiong *et al.* [26] studied the Fischer Tropsch Synthesis over cobalt catalyst and reported that large gamma alumina pore size resulted in large Co_3O_4 crystalline size [24, 25]. The support nature affects the catalyst characterization and can increase the catalyst activity. Chain growth and site time yields on the supported cobalt catalysts are independent from the alumina support density and also the cobalt dispersion.

Consequently, from the number of cobalt atoms exposed on the surface the catalyst, productivity can be easily evaluated. Iglesia *et al.* [27] found constant site time yield for the cobalt particle size range 10-210 nm, which includes most of the typical low dispersion cobalt Fischer Tropsch catalysts. It is necessary to mention that the effect of support material on the product selectivity is not well

recognized. Iglesia *et al.* [28] postulated that differences in selectivity perceived for cobalt on different supports are due to variations in the extent of α olefin readsorption. Support, dispersion and bimetallic effects are not assumed to affect the probability of essential chain growth on the cobalt catalyst surface.

Cobalt dispersion, stability and reducibility are considered as the main factors affecting the catalytic performance. Cobalt supported on alumina catalysts were prepared via incipient wetness impregnation with a solution of cobalt nitrate. Then, supported cobalt catalysts were decomposed by drying and calcination process. Finally catalysts were reduced by flowing hydrogen to achieve metallic cobalt which is necessary to obtain the active sites for the reaction. The procedure which is used for the catalyst preparation and any required characterization process, optimized to attain desirable cobalt alumina catalyst for Fischer Tropsch Synthesis process [27].

2 Experimental

2.1 Catalyst Preparation

Alumina was selected as a catalyst's support due to its appropriate mechanical properties. Alumina support which was used for this experiment has the BET surface area of 98.17 m^2g^{-1}, Pore Volume 0.24 Cm^3g^{-1} and an average pore diameter of 9.9 nm with cylindrical shape (pellet). Cobalt catalysts were prepared via one step incipient wetness impregnation using ethanol (C_2H_5OH) solutions of Cobalt II Nitrate Hexahydrate ($Co(NO_3)_2.6H_2O$), (2.06 Molar); also distilled water was used to compare their results and select an appropriate solution. To investigate the effect of the impregnation on the crystallite size, surface area and also the cobalt content, three different impregnation methods with various durations were investigated. In these methods alumina was impregnated for 2, 6 and 15 hours. The impregnated catalysts were dried at 120°C (5 hours, heating ramp 5° C∘min^{-1}) and calcined at 400°C (10 hours, heating ramp 5 ° C∘min^{-1}). The cobalt content of the catalysts was 7.33 wt.% 11.20 wt.% and 14.48 wt.% respectively. The third catalysts were characterized by several characterization techniques to obtain a desirable cobalt catalyst for FTS experiment.

2.2 Catalyst Characterization

The most common methods of catalyst characterization were:

- Nitrogen adsorption/desorption
- X-ray diffraction (XRD)
- X-ray fluorescence (XRF)
- Scanning electron microscopy (SEM)
- Energy dispersive spectroscopy (EDS),
- Temperature programmed reduction (TPR)
- Temperature programmed desorption (TPD)
- CO-pulse chemisorption
- Temperature programmed oxidation (TPO).

2.2.1 Nitrogen adsorption /desorption

Nitrogen adsorption/desorption isotherms were measured on Micromeritics ASAP 2010 and the data was collected at a liquid nitrogen constant nitrogen temperature (–196°C). The support and prepared catalysts were compared by this test to investigate the change of BET surface area and pore volume after impregnation. Alumina support and cobalt catalyst samples (1.043 g and 2.16 g) were degassed at 300°C for measurement. Brunauer-Emmett-Teller (BET) method is employed to explain the physical adsorption of nitrogen molecule as the most common adsorbate (Gas: N_2, Temperature: –195.8°C, α factor × 105: 6.581/mm Hg, cross sectional area: 0.1620 nm^2) on catalyst surface. This technique is an important analysis method to measure the specific surface area, pore diameter of the catalyst while the total pore volume and pore size distribution were found applying the Barret-Joyner-Halenda (BJH) method; then results were compared to investigate the change of surface area after impregnation [24].

2.2.2 X-ray diffraction (XRD)

X-ray diffraction patterns of all catalysts were recorded at ambient temperature with a Bruker D8 FOCUS with Cu Kα radiation. For measurement all samples were crushed. XRD scans recorded in 2θ range from 10° to 90° using step size of 0.04Åand step time of 15 s. According to Scherrer's equation [24] average Co_3O_4 crystallite thickness size was calculated with peak located at 2θ = 38.90° in the formula a K factor was considered as 0.89 [24]. The diameter of a given Co_3O_4 particle in which it was assumed to be spherical particles, could be obtained for calculation of metallic

*Co*crystallite by using equation 4.

$$d_{Co} = 0.75\, d_{Co_3O_4} \quad (4)$$

2.2.3 X-ray fluorescence (XRF)

To investigate elemental and oxides analysis of the cobalt catalysts XRF was done by using a Bruker S8 TIGER X-ray spectrometer. Chemplex X-ray additive (81.2% C, 8.1% H, 9.6% O, 1.1% B), (20 wt.% of the sample weight) was added to the sample to attain a uniform size and homogenous distribution forming for X-ray fluorescence analysis. Impurities in the crystals were gained by X-ray fluorescence in operation of spectrometer in standard fewer modes with coverage of a full element. The amount of any elements and oxides particles was detected by the XRF experiment.

2.2.4 Scanning electron microscopy (SEM) and energy dispersive spectroscopy (EDS)

Scanning electron microscopy (SEM) with energy dispersive spectroscopy (EDS) was used to analyze the morphological and micro chemical properties of the catalyst. Jeol 6060 with Oxford Inca EDS was used to investigate the catalyst's elements repartition. Additionally, due to the quantitative and qualitative information, SEM has ability to show different chemical elements repartition in the catalyst matrix. The Structure of the cobalt catalysts at Micro and Nano scale range was investigated by SEM-EDS. Chemical composition between the catalyst grains and inside a catalyst grain was determined.

2.2.5 Temperature programmed reduction (TPR)

TPR determines the number of the reducible species present in the cobalt catalyst and reveals the temperature at which the catalyst was reduced. One of the important aspects of TPR analysis is that the samples do not need to have any special characteristics other than containing reducible metals. Micromeritics Auto Chemisorption II analyzer was used to investigate each 0.2 gram. All catalyst samples were purged with helium at a flow rate of 50 ml·min^{-1} then it was exposed to hydrogen (10% hydrogen in Argon; flow rate 50 ml·min^{-1}) and heated in 5 steps; from ambient to 150°C, 150°C to 235°C, 235°C to 300°C, 300°C to 670°C and finally from 670°C to 800°C at a ramp rate of 10°C·min^{-1}, with a hold time of 15 minutes in all steps. From the hydrogen consumption under the assumption that all cobalt oxide was present as Co_3O_4 the degree of reduction was calculated [29].

2.2.6 Temperature programmed desorption (TPD)

An auto Chemisorption II analyzer was used for TPD testing. Temperature programmed desorption determines the number; type and strength of active sites available on the surface of a catalyst by measuring the amount of gas desorbed at various temperatures. The 0.2 gram samples were used in the analyzer to recognize the different desorption conditions of Tert-Butylamine ($(CH_3)_3CNH_2$) at different temperature and it effects at the surface of alumina. Before test, samples were treated for only 2 minutes in a flow of Helium (Flow rate = 50 ml·min^{-1}) with an increasing temperature from ambient to 40°C; then prepared samples was heated in four steps: from 40°C to 150°C, 150°C to 250°C, 250°C to 370°C and finally from 370°C to 500°C at a ramp rate of 10°C·min^{-1}, with a hold time of 30 minutes in all steps.

2.2.7 CO-pulse chemisorption

By pulsing carbon monoxide over the reduced catalyst the cobalt dispersion percentage was determined. CO-pulse Chemisorption was done by using an auto Chemisorption II analyzer. Pulse Chemisorption analysis determines active surface area, percent metal dispersion and the average active particle size by applying measured doses of carbon monoxide gas to the sample. 0.2 gram of the catalysts was put into a quartz tube. The tube was the put in a temperature controlled oven which was connected to a thermal conductivity detector (TCD). The catalyst was reduced in a flow of hydrogen, and then the sample was purged with helium at 430°C for 2 hours and finally cooled down to room temperature. Carbon monoxide was pulsed at 35°C over the catalyst sample until TCD signal peaks was constant.

2.2.8 Temperature programmed oxidation (TPO)

Temperature programmed oxidation was performed with the AutoChem II. 0.2 gram catalysts samples were reduced (in the TPR experiment). After reduction the samples were put into an air tight oven which was then filled with helium. The oven was heated to 400°C at a rate of 10°*C* per minute. At the final stage when the temperature has reached to 400°C, oxygen was passed through the sam-

ples. From the number of pulses which were reacting with the catalysts samples and the known pulse volume, the amount of oxygen consumed by the catalysts samples was calculated.

3 Results and Discussion

3.1 Nitrogen adsorption/desorption

Table 1 shows the BET surface area, average pore volume and pore diameter by BJH method for narrow pore size alumina pellet support (NPAP) and support impregnated with cobalt solution (Co/NPAP). As shown in this table, the average pore volume for un-impregnated support was 0.24 $cm^3 \cdot g^{-1}$ whereas after impregnation this parameter had been reduced by 12.5% to 0.21 $cm^3 \cdot g^{-1}$. There were also other physical parameters reduced due to catalyst preparation procedures. The reduction in BET surface area was 16.2%. It was concluded that BET surface areas and also pore volume of the alumina support have not changed dramatically by impregnation with cobalt so the alumina support pores were not obstructed by cobalt.

3.2 X-ray diffraction (XRD)

X-ray diffraction patterns of alumina support confirmed the existence of only γ-Al_2O_3. After impregnation the XRD patterns illustrated the reflection of Co_3O_4. Alumina support and cobalt catalyst XRD patterns are shown in Figure 1. As shown in this figure, there is very little difference between impregnated and un-impregnated samples. The impregnated sample was too low to give detectable peaks. The XRD patterns only show the Co_3O_4 peak which is the only detectable crystalline cobalt molecule. The only difference between the X-ray patterns of samples is the width of the Co_3O_4 peaks which means that its crystallite size was dependent on the alumina support. The Co_3O_4 crystallite size was calculated from the Sherrer's formula reflection at 2θ = 38.90° which is presented in Table 1. The average diameter of the cobalt oxide crystallite in cobalt alumina supported catalyst (14.48 wt.%) which was calculated as 46 nm was in good agreement with the pore diameter of alumina support, approximately 38 nm. Bezemer *et al.* and Borg *et al.* [24] concluded that larger cobalt particle size will cause higher activity in FTS than smaller particles. Marie *et al.* [30] concluded that the average diameter of the cobalt oxide crystallite increases by increasing the amount of cobalt content. Xiong *et al.* [26] concluded

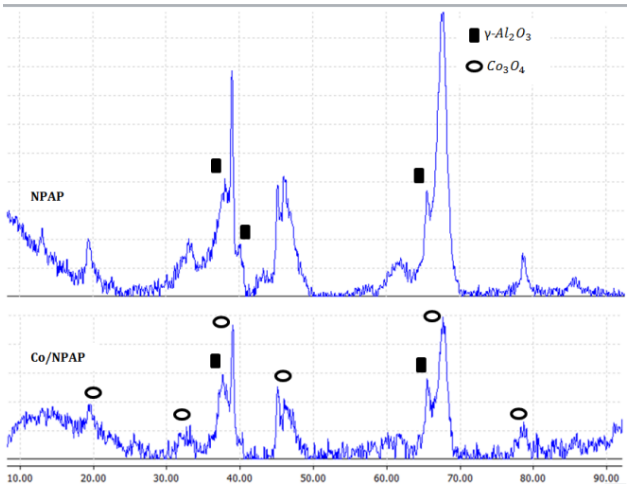

Figure 1: X-ray diffraction patterns of NPAP and Co/NPAP

that Co_3O_4 crystallite size was controlled by the alumina support pore size; so by increasing the alumina support pore diameter, the Co_3O_4 crystallite size increased. Borg *et al.* [31] studied the effect of water on cobalt supported catalyst on FTS process and concluded that cobalt catalyst over narrow pore alumina support provides largest Cobalt (II, III) oxide (Co_3O_4) crystalline size.

3.3 X-ray fluorescence (XRF)

X-Ray Fluorescence (XRF) scans were performed to determine the cobalt elements and oxides contents of the catalyst. Table 2 shows the results of XRF scan. The results shows 14.48 wt.% of cobalt contents in one step impregnation of alumina support with ethanol solution of cobalt (II) nitrate hexahydrate with duration of 15 hours. The cobalt contents was 18.9 wt.% after reduction of catalyst sample from XRF scan. This result shows the efficiency in impregnation of the support in one step impregnation. Also the results of the impregnation for the water solution, which was done previously, were 4% which is not comparable with this cobalt content in Table 2.

Table 2 indicates the different cobalt contents obtained for different impregnation lengths to find an appropriate preparation method.

3.4 Scanning electron microscopy (SEM) and energy dispersive spectroscopy (EDS)

Figure 2 shows Scanning electron microscopy (SEM) images of impregnated alumina pellet with cobalt solution (Co/NPAP). Poly-dispersed spherical particles can be ob-

Table 1: Nitrogen Adsorption data (BET, BJH) for the narrow pore alumina support and impregnated samples with cobalt solution. Experimental Error: BET surface area: ±0.17 m^2g^{-1}, pore volume: ±0.03 cm^3/g and pore diameter: ±0.6 nm / XRF oxide and element results/XRD Co crystallite size/Cobalt Dispersion from CO pulse experiment.

	BET Surface Area (m^2/g)	External Surface Area (m^2/g)	Pore Volume (cm^3/g)	Average Pore Diameter (nm)	XRF Al element wt.%	XRF Co element wt.%	XRF Al_2O_3 wt.%	XRF CoO wt.%	Average SEM-EDS Cobalt %	Co dispersion D_{Co}%	XRD Co_3O_4 Crystallite Size (nm)
NPAP	98.1	95.9	0.24	9.9	-	-	-	-	-	-	38.32
Co/NPAP	82.2	79.9	0.21	10.5	85.43	14.48	92.94	6.97	8.94	23.66	46.29

Table 2: XRF results for different sample impregnated with cobalt solution in different durations.

Impregnation's duration	Cobalt Element (wt.%)	Cobalt Oxide (wt.%)
2 hrs	7.35	3.14
6 hrs	11.20	5.2
15 hrs	14.48 (18.9*)	6.97
* After Reduction		

Table 3: Energy Dispersive Spectroscopy (EDS) results of sample Co/NPAP, cobalt dispersion and contents at different spectrums.

Elements	Weight %	Atomic %
Spectrum 1		
Al K	89.65	94.98
Co L	10.35	5.02
Totals	100.00	
Spectrum 2		
Al K	91.86	96.10
Co L	8.14	3.90
Total	100.00	
Spectrum 3		
Al K	91.67	96.00
Co L	8.33	4.00
Total	100.00	

served on a micrometric scale in these images. Energy dispersive spectroscopy (EDS) scans were performed to calculate the average content of cobalt on the external surface of the catalyst. Table 3 indicates the result of SEM-EDS analysis at different spectrums.

The average cobalt contents of SEM-EDS result is 8.94 wt.% which is in a good agreement with the cobalt content which seen from the X-Ray Fluorescence (Cobalt contents: 14.48 wt.%). Figure 3 indicates the mapping images of cobalt repartition on the catalyst surface. These images were taken at 100μm and shows uniform dispersion of cobalt and alumina. Image 3-b was scanned after 600s. The average atomic ration of sample Co/NPAP is 0.044.

Figure 2 and 3 show that with SEM only large dense mesh of particles of Co compounds can be detected; However with EDS the cobalt particles can be distinguished.

3.5 Temperature programmed reduction (TPR)

In cobalt supported alumina catalyst, the nature and amount of other cations, particularly when cobalt neighbouring with Al cations, influences the reduction temperature of cobalt species as Co has great ability to combine in spinal-like phase. Three categories of interaction between metal oxide and a support can be classified. The first interaction is created when the support acts as a dispersing agent which results in a very weak interaction, second interaction belongs to the formation of solid solution, such as Al_2O_3 and the third one which cobalt supported alumina support is classified in this category is a strong interaction or formation of surface compound [25]. Temperature programmed reduction (TPR) profiles for the sample of the Co/NPAP catalyst is shown in Figure 4. H_2-TPR profile shows three major hydrogen consumption regions. The first reduction step took place at 235°C. At that temperature, un-impregnated residual cobalt nitrate hexahydrate remained after calcination within the support's channels was reduced. This peak is located in a narrow temperature period and did not depend on the physical properties of the catalyst. The second broad peak in profile is related to reduction of Cobalt (II, III) oxide (Co_3O_4) to cobalt oxide (CoO) which is an intermediate between the second and third reduction steps and is depended to physical properties of catalyst such as particle size, surface area and pore volume. Second reduction took place at 300°C and after the second step, cobalt oxide was immediately reduced to Co^0 at 670°C. The catalyst had no further reduction after this temperature. Figure 5 indicates the two step reduction of cobalt oxide species which interact with alumina support (equations 5 and 6). Øyvind Borg *et al.* [24] studied the effect of pore size on cobalt catalyst supported with nar-

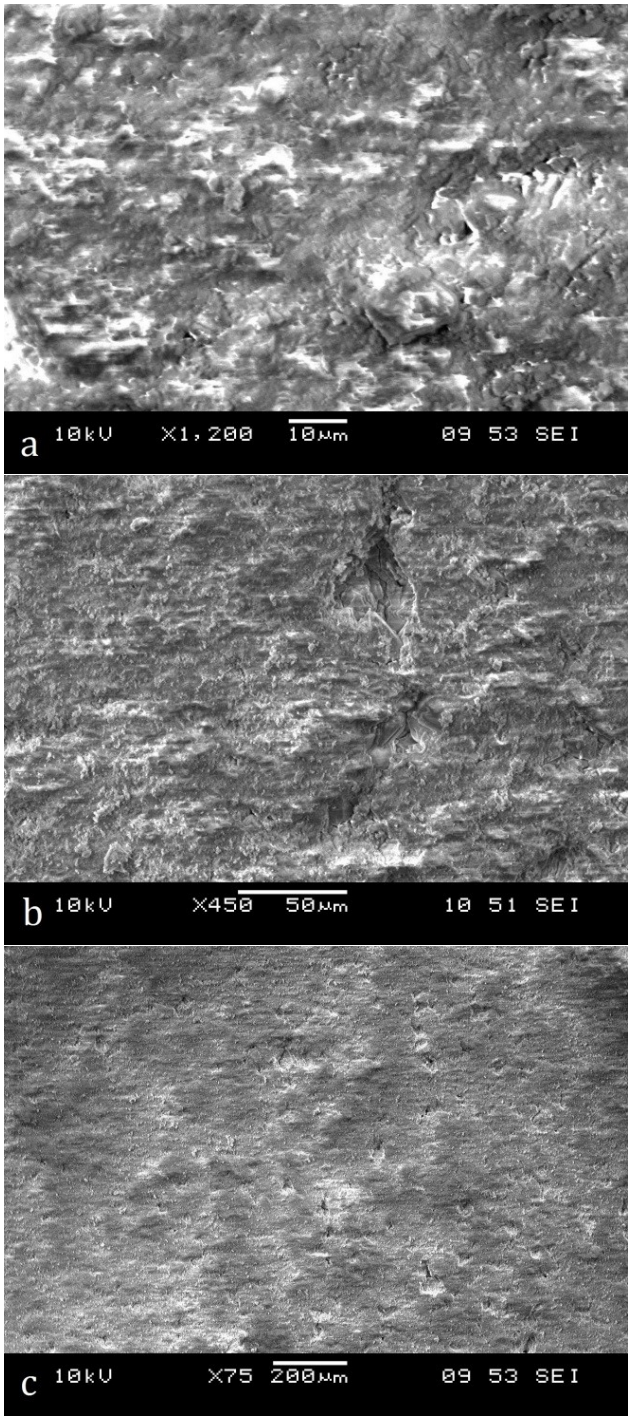

Figure 2: SEM micrographs of Co/NAPA catalyst a) Acc. Volt: 10 kV, 10 µm, b) Acc. Volt: 10 kV, 50 µm, c) Acc. Volt: 10 kV, 200 µm.

row, medium and wide pore volume alumina and reported the same results for H_2-TPR test and concluded that large particle size improved the reducibility of the catalyst.

$$Co_3O_4 + H_2 \rightarrow 3CoO + H_2O \quad (5)$$

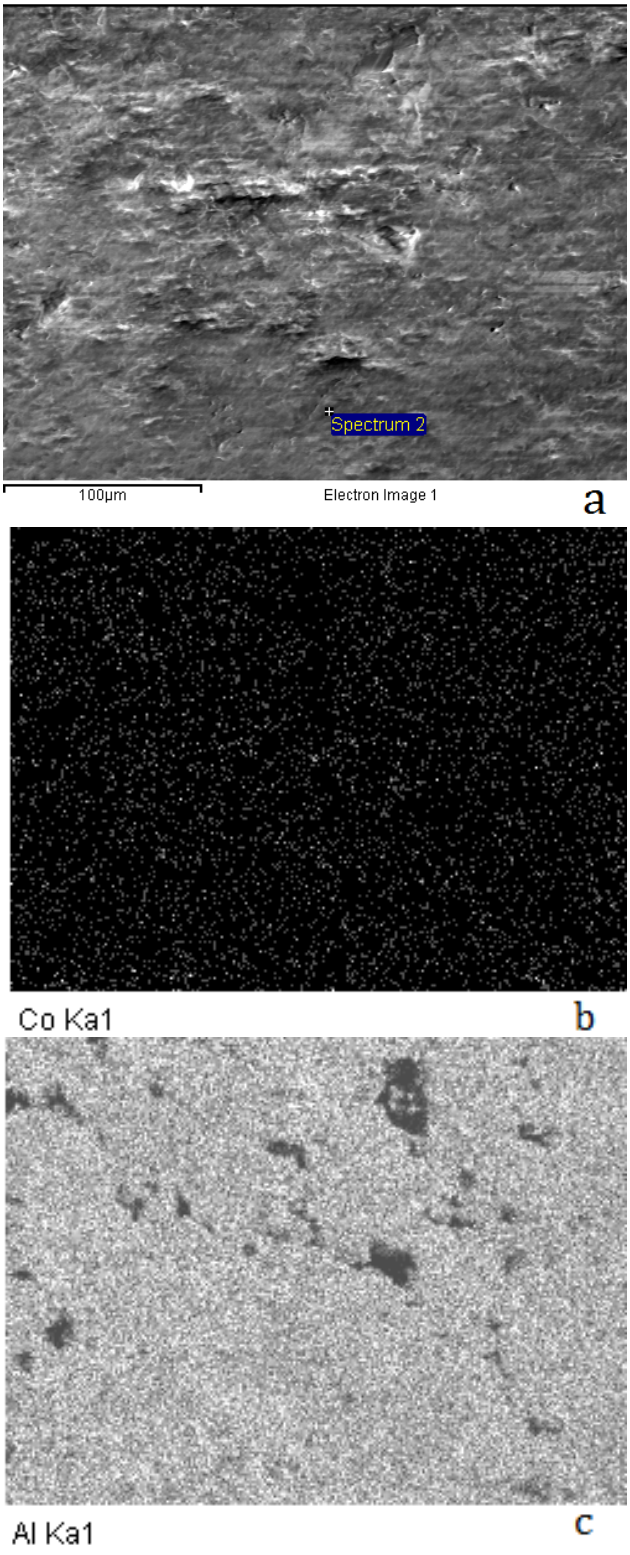

Figure 3: EDS-SEM mapping of surface elements for CO/NPAP sample, a) spectrum 2 at 100µm, b) cobalt repartition on the surface of narrow NPAPA Support, c) repartition of alumina on the surface of the catalyst.

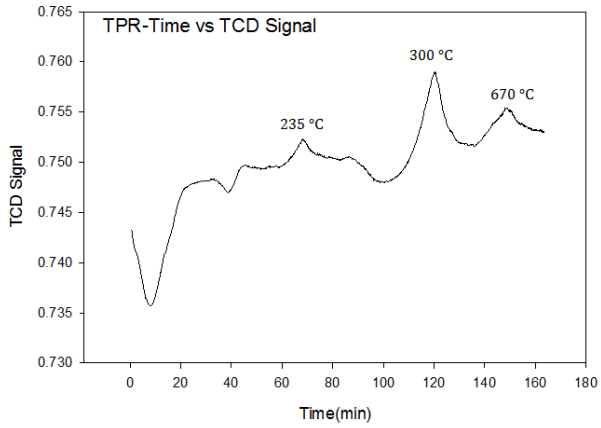

Figure 4: TPR profile for Co/NPAP sample, Different reduction regions at different temperature and time.

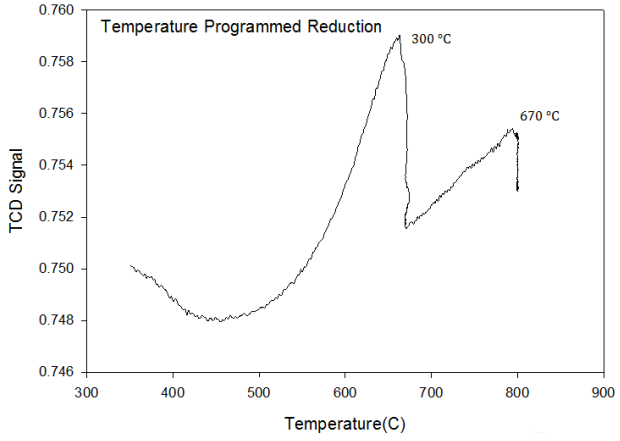

Figure 5: H_2-TPR profile for two step reduction of cobalt oxide species, $Co_3O_4 \rightarrow CoO \rightarrow Co^0$.

$$3CoO + 3H_2 \rightarrow 3Co^0 + 3H_2O \quad (6)$$

3.6 Temperature programmed desorption (TPD)

Temperature programmed desorption (TPD) analysis is employed to determine the number, type, and strength of active sites available on the surface of the cobalt catalyst from measuring the amount of desorbed gas at different temperatures. Figures 6 displays the TPD profile for produced catalyst (Co/NPAP). The first peak introduces the physisorption of tert-Butylamine additionally; the higher area under physisorption peak means more physical adsorption of tert-Butylamine at around 150°C. The second

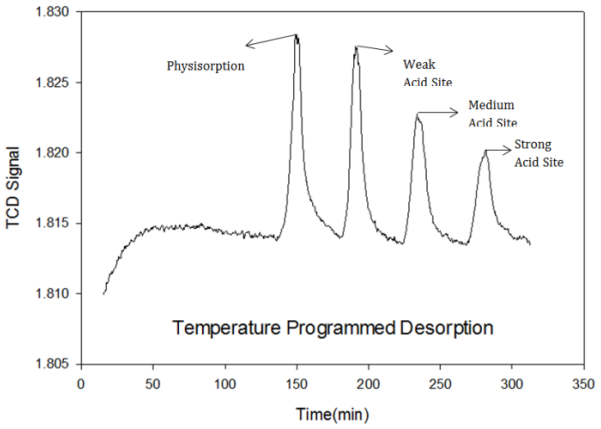

Figure 6: TPD profile for Co/NPAP sample, different desorption regions at different temperature.

peak is related to weak acid site and the higher area under peak for weak acid site means the catalyst is able to produce higher, heavier hydrocarbons. The smaller area under peak for strong acid sites results in the catalyst be deactivated later as catalyst deactivation is one the significant aspects of catalyst preparation.

3.7 Co-pulse chemisorption

For determination of the cobalt dispersion from Co pulse it is required to consider that one carbon monoxide molecule adsorbs only one cobalt species and also, it could neglect the formation of cobalt carbonyls. The cobalt dispersion which was gathered from the AutoChem II analyzer was calculated on the basis of reduced cobalt sites.

Equation 7 indicates cobalt dispersion calculation.

$$D_{Co} = \frac{n_{Co}\ adsorbed\ on\ reduced\ catalyst}{n_{Co} reduced} \times 100 \quad (7)$$

Martin *et al.* [29] calculated the values of cobalt dispersion for alumina supported catalysts between 5 and 9%; however the cobalt dispersion of Co/NAPA which is shown on Table 1 was found to be near 23.66%.

3.8 Temperature programmed oxidation (TPO)

To determine the degree of reduction TPO test were completed to compare with the TPR results. A degree of reduction in TPR and TPO was 47% and 53% respectively which are in very good agreement. Borg *et al.* [24] studied that the oxygen consumption increased with increasing pore and particle size. With BET results which illustrates the

increase in the pore size of the impregnated samples; the oxygen consumption increased strongly.

4 Conclusion

Cobalt catalysts over narrow pore volume alumina support were prepared by one step incipient wetness impregnation of γ-Al_2O_3 with cobalt nitrate hexahydrate ethanol solution. Narrow pore volume alumina was employed to increase the dispersion of the cobalt as it improves the repartition of the cobalt precursor over alumina support. The effect of water and ethanol as solvents were investigated and it was evident that the ethanol improves the formation of cobalt surface phase and active metals site which strongly interacts with alumina. The XRF scan results show 14.48 wt.% cobalt over alumina and 18.9 wt.% after reduction of cobalt by flushing hydrogen which makes this preparation method more efficient. SEM-EDS characterization indicates a uniform dispersion of cobalt over support. The average cobalt content of EDS-SEM characterization shows an average of 8.94 wt.% cobalt repartition, which is in good agreement with XRF results. The catalyst was characterized by CO Pulse experiment which shows the number of reduced cobalt site accessible by pulsing carbon monoxide over the freshly reduced catalyst and shows much higher dispersion of active cobalt (23.66%) in comparison with references. XRD characterization was carried out to calculate the particle size of cobalt crystalline and is with good agreement with crystalline size reported by Jean-Marie. XRD characterization was completed to evaluate the effect of impregnation by ultrasonic mixer and it has been concluded that ultrasonic mixer does not have a significant influence on the crystalline size of catalyst. Bezemer *et al.* found that higher cobalt particle size causes higher activity in FTS experiment. A TPR profile indicates the reduction temperature steps of calcined catalyst. TPD results indicate the physical adsorption of tert-Butylamine at around 200°C which is the active cobalt surface. All cobalt catalyst properties which were compared with mentioned references indicate the desirable prepared catalyst for FTS experiments.

Abbreviations

ASF Anderson-Schulz-Flory
BET Brunauer Emmett Teller
BJH Barret-Joyner-Halenda
BTL Biomass To Liquid
CSA Gas molecular Cross Sectional Area
EDS Energy Dispersive Spectroscopy
FTS Fischer Tropsch Synthesis
FWHM Full Width at Half Max
LPG Liquefied Petroleum Gas
MW Molecular Weight
NPAP Narrow Pore size Alumina Pellet
SEM Scanning Electron Microscopy
TCD Thermal Conductivity Detector
TPD Temperature Programmed Desorption
TPO Temperature Programmed Oxidation
TPR Temperature Programmed Reduction
XRD X-Ray Diffraction
XRF X-Ray Fluorescence
WGSR Water Gas Shift Reaction

Symbols

A_{AB} Pre exponential factor for forward reaction
A_{CS} Adsorbate Cross sectional area (mm^2)
A_f Forward reaction pre exponential factor
A_r Reverse reaction pre exponential factor
C BET Constant
d Cobalt Crystallite Size (nm)
d_t Reactor tube diameter (m)
E_1 Heat of adsorption for the first layer (J)
E_L Heat of liquefaction for higher layers (J)
$\Delta E_{forward}$ Forward reaction activation energy ($kJ{\cdot}mol^{-1}$)
$\Delta E_{reverse}$ Reverse reaction activation energy ($kJ{\cdot}mol^{-1}$)
F_c Calibration Factor
F_0 Flow rate of reactant ($kg{\cdot}m^{-1}$)
h Planck constant
ΔH Enthalpy ($J{\cdot}Kg^{-1}$)
ΔH_R Reaction enthalpy ($kJ{\cdot}mol^{-1}$)
K Sherrer Formula Constant
k_B Boltzmann constant
L_1 Langmuir Surface Area ($g{\cdot}cm^{-3}$)
m Mass of molecule
n Number of carbon
N Avogadro's Number
P Equilibrium pressure of adsorbate Nitrogen at temperature of adsorption (mmHg)
P_0 Saturation pressure of adsorbate Nitrogen at the temperature of adsorption (mmHg)
R Gas constant
R, r_p Rate of reaction ($mol{\cdot}g^{-1}{\cdot}h^{-1}$)
R_I Matrix for reaction rate of terminal gaseous reactants
R_G Matrix of reaction rate of terminal gaseous products
ΔS Entropy ($J{\cdot}K^{-1}$)

T Temperature (K)
T_a Adiabatic temperature (K)
T_P Wall temperature of reactor (K)
U Global heat exchanging coefficient
V/Ng Volume per molecule in the standard state
V_{pa} Peak area volume (cm^3)
W Amount of catalyst (g)
W_n Weight Fraction
x Matrix of surface conversion
α Chain growth probability
θ Matrix of surface coverage
θ_i Angle of incident in XRD (rad)
θ_r Angle of reflection in XRD (rad)
λ Wavelength of X-ray beams (Å)
ρ_A Density of active site ($kg{\cdot}m^3$)
ϵ Void fraction of the catalyst
λ_{er}^{sf} Effective radial thermal conductivity ($W{\cdot}m^{-1}{\cdot}K^{-1}$)

References

[1] D. Dasgupta and T. Wiltowski, Enhancing gas phase Fischer–Tropsch synthesis catalyst design. Fuel, 2011. 90(1): p. 174-181.

[2] D. Tristantini, S. Lögdberg, B. Gevert, Ø. Borg, and A. Holmen, The effect of synthesis gas composition on the Fischer–Tropsch synthesis over Co/γ-Al2O3 and Co–Re/γ-Al2O3 catalysts. Fuel Processing Technology, 2007. 88(7): p. 643-649.

[3] Hessam Jahangiri, James Bennett, Parvin Mahjoubi, Karen Wilson, and S. Gu, A review of advanced catalyst development for Fischer–Tropsch synthesis of hydrocarbons from biomass derived syn-gas. The Royal Society of Chemistry, 2014.

[4] N. Moazami, et al., Modelling of a fixed bed reactor for Fischer–Tropsch synthesis of simulated N2-rich syngas over Co/SiO2: Hydrocarbon production. Fuel, 2015. 154: p. 140-151.

[5] N. Moazami, et al., Catalytic performance of cobalt–silica catalyst for Fischer–Tropsch synthesis: Effects of reaction rates on efficiency of liquid synthesis. Chemical Engineering Science, 2015. 134: p. 374-384.

[6] N. Moazami, et al., Mathematical Modeling and Performance Study of Fischer-tropsch Synthesis of Liquid Fuel over Cobalt-silica. Energy Procedia, 2015. 75: p. 62-71.

[7] H. Mahmoudi, et al., A review of Fischer Tropsch synthesis process, mechanism, surface chemistry and catalyst formulation, in Biofuels Engineering. 2017. p. 11.

[8] O. Doustdar, M.L. Wyszynski, A. Tsolakis, and H. Mahmoudi, Bio-Ketones from lignocellulosic biomass: Experimental investigation on fuel properties, combustion and emission characteristics of cyclopentanone blend with diesel in compression ignition engine. Combustion Engines PTNSS, 2017.

[9] O. Doustdar, M.L. Wyszynski, H. Mahmoudi, and A. Tsolakis, Enhancing the properties of Fischer-Tropsch fuel produced from syngas over Co/SiO2 catalyst: Lubricity and Calorific Value, in IOP Conference Series: Materials Science and Engineering. 2016. p. 012092.

[10] M.R. Hamedi, A. Tsolakis, and J.M. Herreros, Thermal Performance of Diesel Aftertreatment: Material and Insulation CFD Analysis. 2014, SAE International.

[11] S. Zeraati Rezaei, et al., Investigation of two-stage split-injection strategies for a Dieseline fuelled PPCI engine. Fuel, 2013. 107: p. 299-308.

[12] M. Bogarra-Macias, et al., Performance of a drop-in biofuel emulsion on a single-cylinder research diesel engine. Combustion Engines PTNSS, 2016. 166: p. 9-16.

[13] S. Zeng, Y. Du, H. Su, and Y. Zhang, Promotion effect of single or mixed rare earths on cobalt-based catalysts for Fischer–Tropsch synthesis. Catalysis Communications, 2011. 13(1): p. 6-9.

[14] B. Ernst, L. Hilaire, and A. Kiennemann, Effects of highly dispersed ceria addition on reducibility, activity and hydrocarbon chain growth of a Co/SiO2 Fischer–Tropsch catalyst. Catalysis Today, 1999. 50(2): p. 413-427.

[15] H. Mahmoudi, Perfomance of cobalt-based eggshell catalyst in low temperature Fischer tropsch synthesis process to produce long-chain hydrocarbons from synthesis gas utilizing fixed-bed reactor technology, in School of Mechanical Engineering. 2015, The University of Birmingham.

[16] M.H. Rafiq, H.A. Jakobsen, R. Schmid, and J.E. Hustad, Experimental studies and modeling of a fixed bed reactor for Fischer–Tropsch synthesis using biosyngas. Fuel Processing Technology, 2011. 92(5): p. 893-907.

[17] J.H. Yang, et al., Mass transfer limitations on fixed-bed reactor for Fischer–Tropsch synthesis. Fuel Processing Technology, 2010. 91(3): p. 285-289.

[18] E. van Steen and M. Claeys, Fischer-Tropsch Catalysts for the Biomass-to-Liquid (BTL)-Process. Chemical Engineering & Technology, 2008. 31(5): p. 655-666.

[19] R. Guettel and T. Turek, Comparison of different reactor types for low temperature Fischer–Tropsch synthesis: A simulation study. Chemical Engineering Science, 2009. 64(5): p. 955-964.

[20] Y.H. Kim, K.-W. Jun, H. Joo, C. Han, and I.K. Song, A simulation study on gas-to-liquid (natural gas to Fischer–Tropsch synthetic fuel) process optimization. Chemical Engineering Journal, 2009. 155(1): p. 427-432.

[21] R.B. Anderson, The Fischer Tropsch Synthesis. Department of Chemical Engineering: McMaster University, Hamilton, Ontario, Canada.

[22] M.E. Dry, The Fischer–Tropsch process: 1950–2000. Catalysis Today, 2002. 71(3): p. 227-241.

[23] A.R. de la Osa, A. De Lucas, A. Romero, J.L. Valverde, and P. Sánchez, Influence of the catalytic support on the industrial Fischer–Tropsch synthetic diesel production. Catalysis Today, 2011. 176(1): p. 298-302.

[24] Ø. Borg, et al., Fischer–Tropsch synthesis over un-promoted and Re-promoted γ-Al2O3 supported cobalt catalysts with different pore sizes. Catalysis Today, 2009. 142(1–2): p. 70-77.

[25] Y. Zhang, H. Xiong, K. Liew, and J. Li, Effect of magnesia on alumina-supported cobalt Fischer–Tropsch synthesis catalysts. Journal of Molecular Catalysis A: Chemical, 2005. 237(1): p. 172-181.

[26] H. Xiong, Y. Zhang, S. Wang, and J. Li, Fischer–Tropsch synthesis: the effect of Al2O3 porosity on the performance of Co/Al2O3 catalyst. Catalysis Communications, 2005. 6(8): p. 512-516.

[27] E. Iglesia, Design, synthesis, and use of cobalt-based Fischer-Tropsch synthesis catalysts. Applied Catalysis A: General, 1997. 161(1): p. 59-78.

[28] E. Iglesia, S.L. Soled, and R.A. Fiato, Fischer-Tropsch synthesis on cobalt and ruthenium. Metal dispersion and support effects on reaction rate and selectivity. Journal of Catalysis, 1992. 137(1): p. 212-224.

[29] M. Kraum and M. Baerns, Fischer–Tropsch synthesis: the influence of various cobalt compounds applied in the preparation of supported cobalt catalysts on their performance. Applied Catalysis A: General, 1999. 186(1): p. 189-200.

[30] A. Jean-Marie, A. Griboval-Constant, A.Y. Khodakov, and F. Diehl, Cobalt supported on alumina and silica-doped alumina: Catalyst structure and catalytic performance in Fischer–Tropsch synthesis. Comptes Rendus Chimie, 2009. 12(6–7): p. 660-667.

[31] Ø. Borg, et al., Fischer–Tropsch synthesis over γ-alumina-supported cobalt catalysts: Effect of support variables. Journal of Catalysis, 2007. 248(1): p. 89-100.